

# Dynamical Phase Transition due to Feedback-induced Skin Effect

Ze-Chuan Liu<sup>1</sup>, Kai Li<sup>1</sup>, and Yong Xu<sup>1,2\*</sup>

<sup>1</sup>Center for Quantum Information, IIIS, Tsinghua University, Beijing 100084, People's Republic of China and

<sup>2</sup>Hefei National Laboratory, Hefei 230088, PR China

The non-Hermitian skin effect refers to a phenomenon that eigenstates of a non-Hermitian Hamiltonian mainly reside at a boundary. Remarkably, recent work shows that a similar skin effect can be induced by conditional feedback in a continuously monitored system without the requirement of postselection. Unfortunately, the entanglement phase transition is found to be absent for the late-time steady state. Here, we study the many-body dynamics in a continuously monitored free fermion system with conditional feedback under open boundary conditions. We surprisingly find a novel dynamical phase transition from a logarithmic scaling of the entanglement entropy to an area-law scaling as time evolves. The transition, which is noticeably different from the conventional dynamical phase transition, arises from the competition between the bulk dynamics and boundary skin effects. In addition, we find that while quasidisorder or disorder cannot drive a phase transition for the steady state under open boundary conditions, the transition occurs for the maximum entanglement entropy during the time evolution, which agrees well with the entanglement phase transition for the steady state of the dynamics under periodic boundary conditions.

Non-Hermitian physics has sparked considerable interests from various fields in recent years due to the presence of intriguing phenomena [1–4], such as exceptional points or rings [5–9] and non-Hermitian skin effects [10–16]. In fact, non-Hermiticity is ubiquitous in the dynamics of many-body quantum systems [17]. For instance, when considering postselection in continuous measurements, the many-body dynamics is dictated by a non-Hermitian Hamiltonian [17]. Through non-Hermitian many-body dynamics, many interesting non-equilibrium phenomena have been discovered [18–34]. In particular, it has been found that the steady state of a non-Hermitian dynamics of free fermions in the Hatano-Nelson (HN) model is the skin state where particles mainly reside at a half of a system, possessing an area-law scaling of the entanglement entropy [29]. Later, it was shown that disorder or quasidisorder can drive an entanglement phase transition for the steady state with peculiar scaling properties [35–37].

However, to observe these interesting phenomena, one has to apply postselection, which is formidably challenging for a large system. It is thus urgent to consider a more practical system without the requirement of postselection. In this context, Wang *et al.* studied the dynamics of an open quantum system under continuous measurements and found the absence of the skin states even though a certain trajectory governed by the non-Hermitian Hamiltonian leads to the skin state [38]. Remarkably, with conditional feedback, the late-time steady state always concentrates at an edge, precluding the occurrence of an entanglement phase transition [38, 39]. This is in stark contrast to the measurement-induced phase transition [40–51]. The result may also suggest the absence of disorder-induced entanglement phase transition for the steady state in the system with feedback, in contrast to the non-Hermitian case. This motivates us to ask whether there exist novel phase transitions if we do not focus on the steady states.

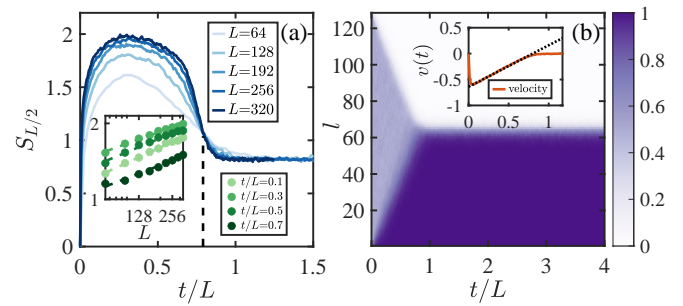


FIG. 1. (a) The time evolution of the trajectory averaged bipartite entanglement entropy  $S_{L/2}$  for different system sizes  $L$  ( $t$  denotes the evolution time). The black dashed line highlights the transition point between the logarithmic-law and area-law regimes. The inset shows the data for several  $t/L$  values in a linear-log scale with  $L$  up to 320, illustrating the log-law scaling. (b) The time evolution of the trajectory averaged density distribution with respect to site  $l$  for a system with  $L = 128$ . Inset: the average velocity  $v(t)$  under OBCs as a function of  $t/L$  (red line). The black dashed line represents a linear fit of  $v(t)$  before the transition point.

In the paper, we study the many-body dynamics of a continuously monitored free fermion system with conditional feedback under open boundary conditions (OBCs). Remarkably, we find the existence of a novel dynamical phase transition from a logarithmic scaling of the entanglement entropy to an area-law scaling with respect to  $t/L$  where  $t$  is the evolution time and  $L$  is the system size (see Fig. 1), although the late-time states approach the skin state even in the presence of strong quasidisorder [see Fig. 3(d)]. The dynamical phase transition arises due to the competition between the bulk dynamics and the dynamics significantly affected by edges. The competition can also be seen from the fact that this dynamical phase transition does not happen under periodic boundary conditions (PBCs). It is important to note that this

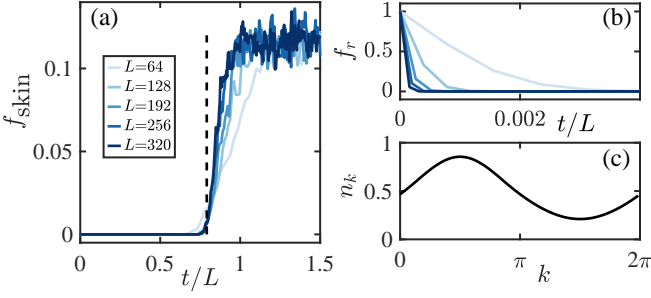


FIG. 2. The time evolution of (a) the probability  $f_{\text{skin}}$  of the evolving state  $|\psi_t\rangle$  being in an ideal many-body skin state  $|\psi_{\text{skin}}\rangle$  and (b) the return probability  $f_r$  for different system sizes averaged over trajectories. In (b), we consider 96 trajectories. The black dashed line marks out the transition point estimated in Fig. 1(a). (c) The density distribution with respect to the momentum  $k$  for the steady state of the dynamics under PBCs with  $L = 128$ .

phase transition is fundamentally different from the traditional dynamical phase transition where the rate function of the Loschmidt echo exhibits a non-analytical behavior [52–56]. In our case, instead of the return probability, the probability for the evolving state to be found in an ideal many-body skin state exhibits a sharp rise across the transition point. In addition, we investigate whether quasidisorder can induce an entanglement phase transition under OBCs in this system. We find that for the late-time steady state, the transition does not happen. However, we show that the dynamics at earlier times is mainly governed by the bulk, resulting in a rapid growth of the entanglement entropy. Later, the entanglement entropy reaches a maximum followed by a decline to a stable value due to the strong boundary effects caused by skin effects. Remarkably, we find that these maximum entanglements undergo a transition from a logarithmic to an area-law scaling as we raise the quasidisorder strength. The results agree well with the transition observed for the steady states under PBCs.

*Trajectory evolution.*— We start by considering a spinless fermion chain of length  $L$  with nearest-neighbor hopping and an onsite quasiperiodic potential described by the Hamiltonian,

$$\hat{H} = \sum_l \left( J(\hat{c}_l^\dagger \hat{c}_{l+1} + \text{H.c.}) + W \cos(2\pi\alpha l) \hat{c}_l^\dagger \hat{c}_l \right), \quad (1)$$

where  $\hat{c}_l^\dagger$  ( $\hat{c}_l$ ) is the creation (annihilation) operator of a fermion at site  $l$ ,  $J$  denotes the hopping strength (we set  $J = 1$  as units of energy hereafter), and  $W$  represents the amplitude of the potential, which is quasiperiodic when  $\alpha$  takes irrational values (we consider  $\alpha = (\sqrt{5} - 1)/2$  without loss of generality). To generate skin effects, we follow Refs. [38, 39] to introduce continuous measurements with feedback represented by the quantum jump operator  $\hat{L}_l = e^{i\theta n_{l+1}} \hat{d}_l^\dagger \hat{d}_l$  with the strength proportional

to  $\gamma$ , where  $\hat{n}_l = \hat{c}_l^\dagger \hat{c}_l$ ,  $\hat{d}_l = \frac{1}{\sqrt{2}}(\hat{c}_l + i\hat{c}_{l+1})$ , and  $\theta$  is a parameter that takes real values (we set  $\theta = \pi$  hereafter). The evolution trajectory of a pure state  $|\psi_t\rangle$  at time  $t$  is then described by a stochastic Schrödinger equation (SSE) [17, 57],

$$d|\psi_t\rangle = -i\hat{H}_{\text{eff}}|\psi_t\rangle dt + \sum_l \left( \hat{L}_l / \sqrt{a_0} - 1 \right) |\psi_t\rangle dW_l, \quad (2)$$

where  $\hat{H}_{\text{eff}} = \hat{H} - i\frac{\gamma}{2} \sum_l \hat{L}_l^\dagger \hat{L}_l$  is the effective Hamiltonian,  $a_0 = \langle \psi_t | \hat{L}_l^\dagger \hat{L}_l | \psi_t \rangle$ , and  $\{dW_l\}$  denotes a set of Poisson random numbers that take the values of either 0 or 1 with the mean value of  $d\bar{W}_l = \gamma a_0 dt$ . Without loss of generality, we take  $\gamma = 0.5$  for all subsequent calculations. Physically,  $\hat{H}_{\text{eff}}$  realizes the HN model if we apply postselection so that the steady state for the system under OBCs is the skin state with electrons mainly occupying part of the system near a boundary [29]. However, postselection is extremely hard for a large system. Unfortunately, without applying postselection, when  $\theta = 0$ , the steady state is not the skin state. Remarkably, it is shown that when  $\theta \neq 0$  (e.g.,  $\theta = \pi$ ), the steady state is always the skin state for a system under OBCs since the detected right-moving particles will be converted to the left-moving one through the imposed phase [38, 39].

To study the dynamical phase transition, we initialize the system in the Neél state, that is,  $|\psi_0\rangle = \prod_{l=1}^{L/2} \hat{c}_{2l}^\dagger |0\rangle$ , where  $|0\rangle$  is the vacuum state. We then numerically calculate each trajectory of  $|\psi_t\rangle$  by solving Eq. (2). The observables are calculated in each trajectory at every time slice, and then averaged over all trajectories. Given that the effective Hamiltonian is quadratic and the jump operators have a simple form, the dynamics could be efficiently simulated with a Slater determinant state [57]. Furthermore, the Gaussian structure of the states allows for the extraction of observables from the correlation matrix  $C_{ij}(t) = \langle \psi_t | \hat{c}_i^\dagger \hat{c}_j | \psi_t \rangle$ . To capture the entanglement phase transition, we focus on the von Neumann entanglement entropy calculated by [58],

$$S_A = -[\text{Tr}(C_A \log C_A + (1 - C_A) \log(1 - C_A))], \quad (3)$$

where  $C_{A,mn} = \langle \hat{c}_m^\dagger \hat{c}_n \rangle$  with  $m, n \in A$  represents the correlation matrix of a subsystem  $A$  of an evolving state. Hereafter, we use  $[\dots]$  to denote the average over trajectories (our numerical results are averaged over 180-2000 trajectories unless stated otherwise) and use  $S_{L/2}$  to denote the entanglement entropy of the left bipartition of the chain.

*Dynamical phase transition without quasidisorder.*— We now investigate the entanglement phase transition that occurs during dynamics for a system under OBCs without quasidisorder (i.e.,  $W = 0$ ). To compare the dynamics of systems with different sizes  $L$ , we rescale the time  $t$  to  $t/L$ . Remarkably, we find that the trajectory averaged entanglement entropy  $S_{L/2}$  undergoes a

phase transition from a log-law to an area-law regime at  $t_c/L \approx 0.79$  as shown in Fig. 1(a). Specifically, as time evolves,  $S_{L/2}$  first increases, then decreases, and eventually reaches a steady value, which is independent of system sizes. The log-law scaling before the phase transition is shown in the inset of Fig. 1(a).

To explain the behavior of  $S_{L/2}$ , we examine the evolution of the density distribution  $[\langle \hat{n}_l \rangle]$ . As shown in Fig. 1(b), all particles move to the left side of the chain and eventually populate the left part. This phenomenon is a result of the feedback-induced skin effect, which has been discussed in Refs. [38, 39]. By comparing the evolution of  $S_{L/2}$ , we observe that before all particles reach the left side,  $S_{L/2}$  increases with increasing  $L$ . Once the state  $|\psi_t\rangle$  becomes a skin state,  $S_{L/2}$  no longer grows.

We note that this dynamical phase transition is different from the conventional one that exhibits singularities in the rate function of the Loschmidt echo at the transition point [54]. In our dynamics, the return probability  $f_r = [\langle \psi_0 | \psi_t \rangle]^2$  suddenly drops to zero at a very short time as shown in Fig. 2(b). Interestingly, we find that the probability  $f_{\text{skin}} = [\langle \psi_{\text{skin}} | \psi_t \rangle]^2$  of the evolving state being in an ideal many-body skin state  $|\psi_{\text{skin}}\rangle = \prod_{l=1}^{L/2} \hat{c}_l^\dagger |0\rangle$  experiences a sudden rise at the transition point [Fig. 2(a)], indicating that the skin state develops through a phase transition.

We expect that the dynamical phase transition arises from the competition between the dynamics under PBCs and boundary skin effects. At earlier times, since most particles are far away from a boundary, their time evolution is mainly governed by the system under PBCs. However, as time progresses, particles approach a boundary so that the boundary effect becomes relevant.

To demonstrate the competition, we analyze the average velocity per particle  $v(t) = d[\langle \hat{x} \rangle]/dt$  under OBCs where  $[\langle \hat{x} \rangle] = 2 \sum_l l [\langle \psi_t | \hat{n}_l | \psi_t \rangle]/L$  is the average position of the particles [57]. If we assume that the velocity of a single left-moving particle is  $v_0$ , then a fraction of  $2|v_0|t/L$  fermionic particles will reach the left side at time  $t$  ( $t < t_c$ ). As a result, only the remaining particles contribute to the velocity. The average velocity before the transition is thus given by

$$v(t) = (1 - 2|v_0|t/L) v_0. \quad (4)$$

We plot  $v(t)$  in the inset of Fig. 1(b), where the black dashed line represents a linear fit of the data. The slope of the line is determined to be  $2v_0^2 = 0.801$ , from which we obtain  $v_0 = -0.633$ . Since the particles with the velocity  $v_0$  are within the bulk, their properties (including velocities) should be determined by the system under PBCs as we have expected. We now use  $v_0 = (2/L) \sum_k n_k v_k$  to estimate  $v_0$  through pure bulk dynamics. Here,  $v_k = -2 \sin k$  is the group velocity of the HN Hamiltonian at the momentum  $k$ , and  $n_k = [\langle \psi_{\text{steady}} | \hat{c}_k^\dagger \hat{c}_k | \psi_{\text{steady}} \rangle]$  is the density of particles at  $k$  in the steady state  $|\psi_{\text{steady}}\rangle$  of

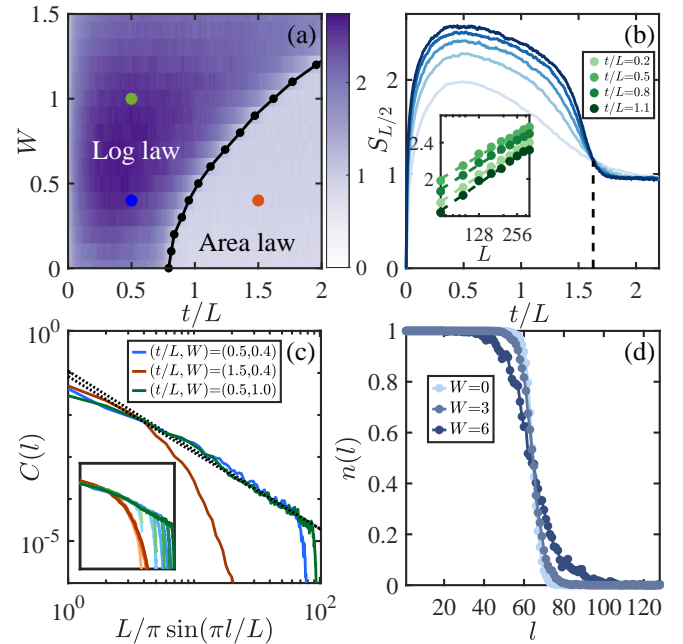


FIG. 3. (a) The phase diagram of the trajectory averaged bipartite entanglement entropy with respect to  $W$  and  $t/L$  with  $L = 320$ . The black line represents the dynamical phase transition line, separating the log-law regime and the area-law regime. (b) The trajectory averaged entanglement entropy  $S_{L/2}$  as a function of  $t/L$  at  $W = 1$ . Inset: the linear-log scale plot of  $S_{L/2}$  versus  $L$  at  $t/L = 0.2, 0.5, 0.8, 1.1$  with a log-law fit (the dashed lines). (c) The correlation functions  $C(l)$  versus  $(L/\pi) \sin(\pi l/L)$  at  $(t/L, W) = (0.5, 0.4), (1.5, 0.4), (0.5, 1.0)$ , which are marked out as solid blue, red and green circles in (a), respectively. Here  $L = 320$ . The inset displays a data collapse for different system sizes  $L = 64, 128, 192, 256, 320$ , with the same axes range as the main plot. (d) The steady-state density distribution  $n(l)$  at  $W = 0, 3, 6$ . The total evolution time is set to 10000 to ensure that the final state reaches the steady state.

the dynamics under PBCs [see Fig. 2(c)]. The estimated velocity  $v_0$  is  $-0.633$ , which is the same as the velocity calculated under OBCs. The critical rescaled time  $t_c/L$  is determined by the fact that all particles move to the left side at this time. Thus,  $t_c/L = 1/(2|v_0|) = 0.79$ , which is in excellent agreement with the results in Fig. 1(a).

*Dynamical phase transition with quasidisorder.*— We now investigate the dynamical entanglement transition that occurs when the quasiperiodic potential is added to the system. By numerically analyzing the entanglement entropy  $S_{L/2}$  at different times and for various values of  $L$  and  $W$ , we map out the phase diagram in Fig. 3(a). We see that as  $W$  increases, the dynamical entanglement transition persists from the logarithmic scaling to the area-law scaling, with the transition point being delayed. Specifically, we plot the evolution of  $S_{L/2}$  for various values of  $L$  when  $W = 1$  in Fig. 3(b), clearly illustrating that  $S_{L/2}$  transitions from the logarithmic scaling [see the inset of Fig. 3(b)] to the area-law scaling. At the

transition point,  $t_c/L \approx 1.63$ , which is larger than the transition point value in the case without quasidisorder. The delayed transition point is attributed to the fact that quasidisorder slows down the particles' motion, but eventually, the particles migrate to the left boundary. In addition, we find that the probability of the evolving state being in an ideal many-body skin state suddenly rises across the transition point [57], similar to the case without disorder.

To further provide evidence for the dynamical phase transition, we calculate the connected density-density correlation function

$$C(l) = [\langle \hat{n}_{L/2} \rangle \langle \hat{n}_{L/2+l} \rangle - \langle \hat{n}_{L/2} \hat{n}_{L/2+l} \rangle] \quad (5)$$

for different values of  $W$  and  $t/L$  and plot them in Fig. 3(c). We see clearly that  $C(l)$  decays algebraically when the point  $(W, t/L)$  falls within the log-law regime, whereas it decays exponentially in the area-law regime. This change in the behavior of  $C(l)$  further reveals the existence of the dynamical phase transition.

*Quasidisorder induced entanglement phase transition.*— Previous studies have shown that disorder or quasidisorder can drive an entanglement phase transition in the steady state of the non-Hermitian Hamiltonian dynamics [35–37]. In our case, we find that the feedback measurement dynamics under OBCs always leads to a skin state for the steady state even for a large  $W$  [see Fig. 3(d)], thereby excluding the existence of the phase transition in the steady state. Furthermore, Fig. 4(a) demonstrates that when the quasidisorder is sufficiently strong,  $S_{L/2}$  directly approaches a steady value as time evolves, in contrast to the small  $W$  case where the evolution exhibits a dynamical phase transition, as discussed earlier. In other words, the dynamical phase transition with respect to  $t/L$  disappears for a large  $W$ .

To quantitatively identify the quasidisorder induced disappearance of the dynamical phase transition, we calculate the maximum value  $S_{L/2}^{\max}$  of the entanglement entropy as time evolves at each  $W$  and plot  $S_{L/2}^{\max}$  with respect to  $W$  in Fig. 4(b). The figure shows that  $S_{L/2}^{\max}$  first rises to a peak near  $W \approx 0.8$  and then collapses to the same curve, suggesting the entanglement phase transition from a log-law scaling to an area-law scaling as  $W$  increases [see the inset in Fig. 4(b)]. We find that the transition of  $S_{L/2}^{\max}$  under OBCs reveals the entanglement phase transition in the *steady* state of the dynamics under PBCs [57]. This can be understood from the previous discussion that for weak disorder, at short times before the transition to the area-law regime, the dynamics is mainly governed by the system under PBCs. For strong disorder, since both skin states and localized states respect the area-law entanglement scaling, the entanglement dynamics under OBCs shows a similar growth behavior as its dynamics under PBCs.

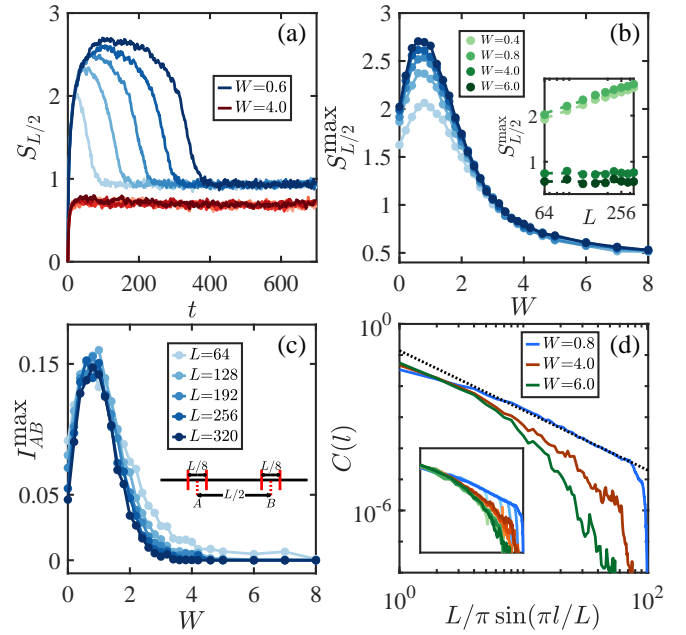


FIG. 4. (a) The time evolution of the trajectory averaged entanglement entropy  $S_{L/2}$  for a system under OBCs with  $L = 64, 128, 192, 256, 320$  (from light to dark colors) at  $W = 0.6$  (blue lines) and  $W = 4$  (red lines). (b) The maximum entanglement entropy  $S_{L/2}^{\max}$  and (c) the maximum mutual information  $I_{AB}^{\max}$  between two subsystems  $A$  and  $B$  with respect to  $W$  for different system sizes. In (c), the inset displays the positions and sizes of the two subsystems. The mutual information is defined as  $I_{AB} = S_A + S_B - S_{A \cup B}$ , where  $S_A$  and  $S_B$  are entanglement entropy of the subsystems  $A$  and  $B$ , respectively, and  $S_{A \cup B}$  is the joint entanglement entropy. In (b) and (c), the maximum value refers to the peak of the corresponding trajectory averaged quantities during time evolution. (d) The correlation function  $C(l)$  versus  $(L/\pi) \sin(\pi l/L)$  at  $W = 0.8, 4, 6$ . The inset displays a data collapse for different system sizes  $L = 64, 128, 192, 256, 320$ .

We further plot the maximum mutual information  $I_{AB}^{\max}$  between two subsystems  $A$  and  $B$  [see the inset of Fig. 4(c)] in the dynamics under OBCs as a function of the quasidisorder strength  $W$  in Fig. 4(c). Similar to the entanglement entropy, we see that  $I_{AB}^{\max}$  first develops a peak near  $W \approx 0.8$  and then declines to zero, providing additional evidence for the quasidisorder induced phase transition. To gain further insights into this transition, we also calculate the correlation function  $C(l)$  of the evolving state at the time when  $S_{L/2}$  reaches its maximum value. We find that for weak disorder, the correlation function exhibits a power-law decay, whereas for strong disorder, it shows an exponential decay [see Fig. 4(d)].

In summary, we have demonstrated a novel dynamical phase transition in the many-body dynamics of a continuously monitored free fermion system with conditional feedback under OBCs. The phase transition manifests in the change in the entanglement scaling, the correla-

tion function and the probability of finding the evolving state in an ideal many-body skin state. We show that the phase transition arises from the competition between the bulk dynamics and boundary skin effects. In addition, we find that while the steady state is still the skin state in the presence of strong quasidisorder, the maximum entanglement exhibits a transition from a logarithmic to an area-law scaling as the quasidisorder strength increases. Since onsite disorder is ubiquitous, we have provided the results for the case with onsite disorder (rather than quasidisorder) in the Supplemental Material [57], showing that the dynamical phase transition persists. Given the rapid progress in quantum simulators, such as trapped ions [59], the novel dynamical phase transitions may be experimentally observed in trapped ions [38].

We thank J.-H. Wang, X. Feng, and S. Liu for helpful discussions. This work is supported by the National Natural Science Foundation of China (Grant No. 11974201), Tsinghua University Dushi Program and Innovation Program for Quantum Science and Technology (Grant No. 2021ZD0301604).

\* [yongxuphy@tsinghua.edu.cn](mailto:yongxuphy@tsinghua.edu.cn)

- [1] R. El-Ganainy, K. G. Makris, M. Khajavikhan, Z. H. Musslimani, S. Rotter, and D. N. Christodoulides, *Nat. Phys.* **14**, 11 (2018).
- [2] Y. Xu, *Front. Phys.* **14**, 43402 (2019).
- [3] Y. Ashida, Z. Gong, and M. Ueda, *Adv. Phys.* **69**, 249 (2020).
- [4] E. J. Bergholtz, J. C. Budich, and F. K. Kunst, *Rev. Mod. Phys.* **93**, 015005 (2021).
- [5] N. Moiseyev, *Non-Hermitian Quantum Mechanics* (Cambridge Univ. Press, 2011).
- [6] B. Zhen, C. W. Hsu, Y. Igarashi, L. Lu, I. Kaminer, A. Pick, S.-L. Chua, J. D. Joannopoulos, and M. Soljačić, *Nature (London)* **525**, 354 (2015).
- [7] Y. Xu, S.-T. Wang, and L.-M. Duan, *Phys. Rev. Lett.* **118**, 045701 (2017).
- [8] D. Leykam, K. Y. Bliokh, C. Huang, Y. D. Chong, and F. Nori, *Phys. Rev. Lett.* **118**, 040401 (2017).
- [9] K. Kawabata, T. Bessho, and M. Sato, *Phys. Rev. Lett.* **123**, 066405 (2019).
- [10] N. Hatano and D. R. Nelson, *Phys. Rev. Lett.* **77**, 570 (1996).
- [11] N. Hatano and D. R. Nelson, *Phys. Rev. B* **56**, 8651 (1997).
- [12] T. E. Lee, *Phys. Rev. Lett.* **116**, 133903 (2016).
- [13] S. Yao and Z. Wang, *Phys. Rev. Lett.* **121**, 086803 (2018).
- [14] Y. Xiong, *J. Phys. Commun.* **2**, 035043 (2018).
- [15] V. M. Martinez Alvarez, J. E. Barrios Vargas, and L. E. F. Foa Torres, *Phys. Rev. B* **97**, 121401(R) (2018).
- [16] F. K. Kunst, E. Edvardsson, J. C. Budich, and E. J. Bergholtz, *Phys. Rev. Lett.* **121**, 026808 (2018).
- [17] H. M. Wiseman and G. J. Milburn, *Quantum Measurement and Control* (Cambridge University Press, Cambridge, England, 2010).
- [18] Y. Ashida and M. Ueda, *Phys. Rev. Lett.* **120**, 185301 (2018).
- [19] R. Hamazaki, K. Kawabata, and M. Ueda, *Phys. Rev. Lett.* **123**, 090603 (2019).
- [20] M. Nakagawa, N. Tsuji, N. Kawakami, and M. Ueda, *Phys. Rev. Lett.* **124**, 147203 (2020).
- [21] X. Chen, Y. Li, M. P. A. Fisher, and A. Lucas, *Phys. Rev. Research* **2**, 033017 (2020).
- [22] Á. Bácsi and B. Dóra, *Phys. Rev. B* **103**, 085137 (2021).
- [23] S. Gopalakrishnan and M. J. Gullans, *Phys. Rev. Lett.* **126**, 170503 (2021).
- [24] X. Turkeshi, A. Biella, R. Fazio, M. Dalmonte, and M. Schiró, *Phys. Rev. B* **103**, 224210 (2021).
- [25] A. Biella and M. Schiró, *Quantum* **5**, 528 (2021).
- [26] S.-K. Jian, Z.-C. Yang, Z. Bi, and X. Chen, *Phys. Rev. B* **104**, L161107 (2021).
- [27] T. Orito and K.-I. Imura, *Phys. Rev. B* **105**, 024303 (2022).
- [28] Y. L. Gal, X. Turkeshi, and M. Schiró, *SciPost Phys.* **14**, 138 (2023).
- [29] K. Kawabata, T. Numasawa, and S. Ryu, *Phys. Rev. X* **13**, 021007 (2023).
- [30] E. Granet, C. Zhang, and H. Dreyer, *Phys. Rev. Lett.* **130**, 230401 (2023).
- [31] X. Turkeshi and M. Schiró, *Phys. Rev. B* **107**, L020403 (2023).
- [32] S. Longhi, *Phys. Rev. B* **108**, 075121 (2023).
- [33] J. Mák, M. J. Bhaseen, and A. Pal, [arXiv:2301.01763](https://arxiv.org/abs/2301.01763).
- [34] T. Orito and K.-I. Imura, [arXiv:2308.03078](https://arxiv.org/abs/2308.03078).
- [35] K. Li, Z.-C. Liu, and Y. Xu, [arXiv:2305.12342](https://arxiv.org/abs/2305.12342).
- [36] S.-Z. Li, X.-J. Yu, and Z. Li, [arXiv:2309.03546](https://arxiv.org/abs/2309.03546).
- [37] L. Zhou, [arXiv:2309.00924](https://arxiv.org/abs/2309.00924).
- [38] Y.-P. Wang, C. Fang, and J. Ren, [arXiv:2209.11241](https://arxiv.org/abs/2209.11241).
- [39] X. Feng, S. Liu, S. Chen, and W. Guo, [arXiv:2212.08090](https://arxiv.org/abs/2212.08090).
- [40] Y. Li, X. Chen, and M. P. A. Fisher, *Phys. Rev. B* **98**, 205136 (2018).
- [41] A. Chan, R. M. Nandkishore, M. Pretko, and G. Smith, *Phys. Rev. B* **99**, 224307 (2019).
- [42] B. Skinner, J. Ruhman, and A. Nahum, *Phys. Rev. X* **9**, 031009 (2019).
- [43] X. Cao, A. Tilloy, and A. D. Luca, *SciPost Phys.* **7**, 024 (2019).
- [44] Y. Li, X. Chen, and M. P. A. Fisher, *Phys. Rev. B* **100**, 134306 (2019).
- [45] S. Choi, Y. Bao, X.-L. Qi, and E. Altman, *Phys. Rev. Lett.* **125**, 030505 (2020).
- [46] O. Alberton, M. Buchhold, and S. Diehl, *Phys. Rev. Lett.* **126**, 170602 (2021).
- [47] T. Minato, K. Sugimoto, T. Kuwahara, and K. Saito, *Phys. Rev. Lett.* **128**, 010603 (2022).
- [48] M. Block, Y. Bao, S. Choi, E. Altman, and N. Y. Yao, *Phys. Rev. Lett.* **128**, 010604 (2022).
- [49] T. Müller, S. Diehl, and M. Buchhold, *Phys. Rev. Lett.* **128**, 010605 (2022).
- [50] X. Yu and X.-L. Qi, [arXiv:2201.12704](https://arxiv.org/abs/2201.12704).
- [51] K. Yamamoto and R. Hamazaki, [arXiv:2301.07290](https://arxiv.org/abs/2301.07290).
- [52] M. Heyl, A. Polkovnikov, and S. Kehrein, *Phys. Rev. Lett.* **110**, 135704 (2013).
- [53] B. Žunkovič, M. Heyl, M. Knap, and A. Silva, *Phys. Rev. Lett.* **120**, 130601 (2018).
- [54] M. Heyl, *Rep. Prog. Phys.* **81**, 054001 (2018).
- [55] A. A. Zvyagin, *Low Temp. Phys.* **42**, 971 (2016).
- [56] B. Žunkovič, A. Silva, and M. Fabrizio, *Phil. Trans. R. Soc. A* **374**, 20150160 (2016).

[57] See the Supplemental Material.  
 [58] I. Peschel, J. Phys. A **36**, L205 (2003).  
 [59] C. Monroe, W. C. Campbell, L.-M. Duan, Z.-X. Gong, A. V. Gorshkov, P. W. Hess, R. Islam, K. Kim, N. M.

Linke, G. Pagano, P. Richerme, C. Senko, and N. Y. Yao, Rev. Mod. Phys. **93**, 025001 (2021).

In the Supplemental Material, we will provide details on how to derive and solve the stochastic Schrödinger equation in Section S-1, show the probability of finding the evolving state in the ideal many-body skin state for a system with quasidisorder in Section S-2, discuss the results of the dynamics of the system under PBCs in Section S-3, and finally present the results of the dynamics of the system with onsite disorder in Section S-4.

### S-1. QUANTUM JUMP EVOLUTION

In the section, we will follow Refs. [17, 38, 39] to derive the stochastic Schrödinger equation for a continuously monitored system and present how we solve the equation to obtain the trajectories for a comprehensive reading. In addition, we provide details on how to calculate the average velocity per particle for a system under OBCs.

#### A. The stochastic Schrödinger equation

To derive the stochastic Schrödinger equation, we consider a system subject to a unitary evolution of a Hamiltonian  $\hat{H}$  and continuous measurements. In each infinitesimal time interval  $[t, t + dt]$ , we first evolve the state of the system  $|\psi(t)\rangle$  by the Hamiltonian  $\hat{H}$ , that is,

$$|\psi(t + dt)\rangle = (1 - i\hat{H}dt)|\psi(t)\rangle. \quad (\text{S1})$$

Subsequently, we perform a measurement on the state  $|\psi(t + dt)\rangle$ . The measurement is described by the following measurement operators,

$$\begin{aligned} \hat{M}_m &= \hat{L}_m \sqrt{\gamma dt} \\ \hat{M}_0 &= \sqrt{1 - \gamma \hat{R}dt} = 1 - \frac{\gamma}{2} \hat{R}dt, \end{aligned} \quad (\text{S2})$$

where  $m = 1, 2, \dots, M$ ,  $\hat{L}_m$  are quantum jump operators,  $\gamma$  is the monitoring rate, and

$$\hat{R} = \sum_{m=1}^M \hat{L}_m^\dagger \hat{L}_m. \quad (\text{S3})$$

In the final step, we have neglected the higher-order contributions in  $dt$ . Clearly, these measurement operators satisfy the completeness equation,  $\sum_m \hat{M}_m^\dagger \hat{M}_m = 1$ .

The post measurement state is governed by a random process. Specifically, through a non-Hermitian evolution, the state will become

$$|\psi(t + dt)\rangle \rightarrow \frac{\hat{M}_0 |\psi(t + dt)\rangle}{\sqrt{\langle \psi(t + dt) | \hat{M}_0^\dagger \hat{M}_0 | \psi(t + dt) \rangle}} = \frac{\hat{U}_0 |\psi(t)\rangle}{\sqrt{\langle \psi(t) | \hat{U}_0^\dagger \hat{U}_0 | \psi(t) \rangle}} = \left( 1 - i\hat{H}_{\text{eff}}dt + \frac{\gamma}{2} \langle \psi(t) | \hat{R} | \psi(t) \rangle dt \right) |\psi(t)\rangle \quad (\text{S4})$$

with the probability of

$$P(0) = \langle \psi(t + dt) | \hat{M}_0^\dagger \hat{M}_0 | \psi(t + dt) \rangle = \langle \psi(t) | \hat{U}_0^\dagger \hat{U}_0 | \psi(t) \rangle, \quad (\text{S5})$$

where  $\hat{U}_0 = \hat{M}_0 - i\hat{H}dt = 1 - i\hat{H}_{\text{eff}}dt$  is the evolution operator and  $\hat{H}_{\text{eff}} = \hat{H} - i\gamma\hat{R}/2$  is the non-Hermitian effective Hamiltonian. Through a jump process, the state can become

$$|\psi(t + dt)\rangle \rightarrow \frac{\hat{M}_m |\psi(t + dt)\rangle}{\sqrt{\langle \psi(t + dt) | \hat{M}_m^\dagger \hat{M}_m | \psi(t + dt) \rangle}} = \frac{\hat{M}_m |\psi(t)\rangle}{\sqrt{\langle \psi(t) | \hat{M}_m^\dagger \hat{M}_m | \psi(t) \rangle}} = \frac{\hat{L}_m |\psi(t)\rangle}{\sqrt{\langle \psi(t) | \hat{L}_m^\dagger \hat{L}_m | \psi(t) \rangle}} \quad (\text{S6})$$

with the probability of

$$P(m) = \langle \psi(t+dt) | \hat{M}_m^\dagger \hat{M}_m | \psi(t+dt) \rangle = \langle \psi(t) | \hat{M}_m^\dagger \hat{M}_m | \psi(t) \rangle. \quad (\text{S7})$$

We now introduce a set of random variables  $\{(dW_1, dW_2, \dots, dW_M) : dW_m \in \{0, 1\}\}$  with  $m = 1, 2, \dots, M$  satisfying  $dW_m dW_n = \delta_{mn} dW_m$  (i.e., there is at most one  $dW_m = 1$ ). The probability that  $dW_m = 1$  is  $\mathbb{E}(dW_m) = P(m) = \langle \psi(t) | \hat{L}_m^\dagger \hat{L}_m | \psi(t) \rangle \gamma dt$ . The random process can be represented by a differential equation,

$$\begin{aligned} |\psi(t+dt)\rangle &= \sum_{m=1}^M dW_m \frac{\hat{L}_m | \psi(t) \rangle}{\sqrt{\langle \psi(t) | \hat{L}_m^\dagger \hat{L}_m | \psi(t) \rangle}} + (1 - \sum_{m=1}^M dW_m) (1 - i\hat{H}_{\text{eff}} dt + \frac{\gamma}{2} \langle \psi(t) | \hat{R} | \psi(t) \rangle dt) | \psi(t) \rangle \\ &= \left(1 - i\hat{H}_{\text{eff}} dt + \frac{\gamma}{2} \langle \psi(t) | \hat{R} | \psi(t) \rangle dt\right) | \psi(t) \rangle + \sum_{m=1}^M dW_m \left( \frac{\hat{L}_m}{\sqrt{\langle \psi(t) | \hat{L}_m^\dagger \hat{L}_m | \psi(t) \rangle}} - 1 \right) | \psi(t) \rangle, \end{aligned} \quad (\text{S8})$$

where we have neglected the higher-order terms in  $dt$ . From Eq. (S8), we have

$$d|\psi(t)\rangle = \left(-i\hat{H}_{\text{eff}} + \frac{\gamma}{2} \langle \psi(t) | \hat{R} | \psi(t) \rangle\right) |\psi(t)\rangle dt + \sum_{m=1}^M dW_m \left( \frac{\hat{L}_m}{\sqrt{\langle \psi(t) | \hat{L}_m^\dagger \hat{L}_m | \psi(t) \rangle}} - 1 \right) |\psi(t)\rangle, \quad (\text{S9})$$

which is the stochastic Schrödinger equation in the main text. The constant term  $\frac{\gamma}{2} \langle \psi(t) | \hat{R} | \psi(t) \rangle$  can be neglected if we enforce  $\langle \psi(t) | \psi(t) \rangle = 1$ .

## B. Numerical simulation of the stochastic Schrödinger equation

For an efficient numerical simulation of the stochastic Schrödinger equation [Eq. (S9)], we use a finite time interval  $\Delta t$  and consider the following dynamics. Given a state  $|\psi(t)\rangle$  at time  $t$ , we first evolve the state using the non-Hermitian effective Hamiltonian  $\hat{H}_{\text{eff}}$ , obtaining

$$|\psi(t + \Delta t)\rangle = \frac{1}{\mathcal{N}} e^{-i\hat{H}_{\text{eff}}\Delta t} |\psi(t)\rangle. \quad (\text{S10})$$

Considering the fact that there can be multiple quantum jumps when the time interval  $\Delta t$  is finite, the measurement process is approximated by [38, 39]

$$|\psi(t + \Delta t)\rangle \rightarrow \frac{1}{\mathcal{N}'} \prod_m \left( \Delta W_m \hat{L}_m + 1 - \Delta W_m \right) |\psi(t + \Delta t)\rangle, \quad (\text{S11})$$

with  $\Delta W_m \in \{0, 1\}$  and  $P(\Delta W_m = 1) = \langle \psi(t) | \hat{L}_m^\dagger \hat{L}_m | \psi(t) \rangle \gamma \Delta t$  (there can be multiple  $\Delta W_m = 1$ ). Here  $\mathcal{N}$  and  $\mathcal{N}'$  are normalization constants to ensure that the states are normalized. We note that when  $\Delta t \rightarrow 0$ , the probability for two or more quantum jumps, which is  $O(\Delta t^2)$ , is negligible compared to the probability for one quantum jump  $O(\Delta t)$ , recovering the original quantum jump evolution [Eq. (S8)].

Since both the non-Hermitian evolution Eq. (S10) and the quantum jumps Eq. (S11) preserve the Slater determinant form, we can represent the state at time  $t$ ,  $|\psi(t)\rangle$  by an  $L \times N$  matrix  $U(t)$ , with  $L$  being the system size and  $N$  being the particle number. Each column of  $U(t)$  corresponds a single-particle state, and the many-body state  $|\psi(t)\rangle$  is given by

$$|\psi(t)\rangle = \prod_{n=1}^N \left( \sum_{i=1}^L [U(t)]_{in} \hat{c}_i^\dagger \right) |0\rangle. \quad (\text{S12})$$

Suppose that the non-Hermitian effective Hamiltonian is written as

$$\hat{H}_{\text{eff}} = \sum_{i,j=1}^L [H_{\text{eff}}]_{ij} \hat{c}_i^\dagger \hat{c}_j, \quad (\text{S13})$$

then the non-Hermitian evolution Eq. (S10) can be efficiently simulated by

$$U(t + \Delta t) = \text{qr}[e^{-iH_{\text{eff}}\Delta t}U(t)], \quad (\text{S14})$$

where qr stands for the QR decomposition to make sure  $|\psi(t + \Delta t)\rangle$  is normalized.

Now, we focus on the simulation of the quantum jump  $|\psi\rangle \rightarrow \hat{L}_l|\psi\rangle/\sqrt{\langle\psi|\hat{L}_l^\dagger\hat{L}_l|\psi\rangle}$ . The jump operator is given by

$$\hat{L}_l = e^{i\pi\hat{n}_{l+1}}\hat{d}_l^\dagger\hat{d}_l, \quad (\text{S15})$$

with  $\hat{d}_l^\dagger = \sum_{i=1}^L [d_l]_i \hat{c}_i^\dagger$  and  $d_l$  being a column vector specified by  $[d_l]_i = \frac{1}{\sqrt{2}}(\delta_{i,l} - i\delta_{i,l+1})$ . Let

$$\hat{\gamma}_n^\dagger = \sum_{i=1}^L U_{in} \hat{c}_i^\dagger, \quad (\text{S16})$$

we have

$$|\psi\rangle = \hat{\gamma}_1^\dagger \hat{\gamma}_2^\dagger \cdots \hat{\gamma}_N^\dagger |0\rangle, \quad (\text{S17})$$

and

$$\hat{d}_l^\dagger \hat{d}_l |\psi\rangle = \langle d_l | \gamma_1 \rangle \hat{d}_l^\dagger \hat{\gamma}_2^\dagger \cdots \hat{\gamma}_N^\dagger |0\rangle + \langle d_l | \gamma_2 \rangle \hat{\gamma}_1^\dagger \hat{d}_l^\dagger \hat{\gamma}_3^\dagger \cdots \hat{\gamma}_N^\dagger |0\rangle + \cdots + \langle d_l | \gamma_N \rangle \hat{\gamma}_1^\dagger \hat{\gamma}_2^\dagger \cdots \hat{\gamma}_{N-1}^\dagger \hat{d}_l^\dagger |0\rangle, \quad (\text{S18})$$

with  $|d_l\rangle = \hat{d}_l^\dagger |0\rangle$  and  $|\gamma_n\rangle = \hat{\gamma}_n^\dagger |0\rangle$ . Without loss of generality, we assume  $\langle d_l | \gamma_1 \rangle \neq 0$ . To simplify this equation, we can perform the following transformation,

$$\hat{\gamma}_n^\dagger \rightarrow \hat{\gamma}'_n^\dagger = \hat{\gamma}_n^\dagger + \left( \delta_{n1} - \frac{\langle d_l | \gamma_n \rangle}{\langle d_l | \gamma_1 \rangle} \right) \hat{\gamma}_1^\dagger. \quad (\text{S19})$$

Equivalently, we have  $U \rightarrow U'$  with

$$U_n \rightarrow U'_n = U_n + \left( \delta_{n1} - \frac{\langle d_l | \gamma_n \rangle}{\langle d_l | \gamma_1 \rangle} \right) U_1, \quad (\text{S20})$$

where  $U_n$  ( $U'_n$ ) is the  $n$ -th column of  $U$  ( $U'$ ). We note that such transformation does not change the many-body state  $|\psi\rangle$  given that  $(\hat{\gamma}_1^\dagger)^2 = 0$ . After the transformation, we have  $\langle d_l | \gamma'_n \rangle = 0$  for  $n \neq 1$ , so

$$\hat{d}_l^\dagger \hat{d}_l |\psi\rangle = \langle d_l | \gamma'_1 \rangle \hat{d}_l^\dagger \hat{\gamma}'_2^\dagger \cdots \hat{\gamma}'_N^\dagger |0\rangle = \langle d_l | \gamma'_1 \rangle \prod_{n=1}^N \left( \sum_{i=1}^L \tilde{U}_{in} \hat{c}_i^\dagger \right) |0\rangle \quad (\text{S21})$$

with

$$\tilde{U} = (d_l \ U'_2 \ U'_3 \ \dots \ U'_n). \quad (\text{S22})$$

We finally arrive at

$$\frac{\hat{L}_l |\psi\rangle}{\sqrt{\langle\psi|\hat{L}_l^\dagger\hat{L}_l|\psi\rangle}} = \prod_{n=1}^N \left( \sum_{i=1}^L \tilde{U}'_{in} \hat{c}_i^\dagger \right) |0\rangle \quad (\text{S23})$$

with  $\tilde{U}' = \text{qr}(e^{i\pi M_{l+1}} \tilde{U})$  and  $[M_{l+1}]_{ij} = \delta_{i,l+1} \delta_{j,l+1}$ .

### C. The average velocity $v(t)$ per particle under OBCs

In this subsection, we will show how to calculate the average velocity  $v(t)$  per particle for a system under OBCs. The velocity under OBCs is defined as

$$v(t) = \frac{d}{dt}[\langle \hat{x} \rangle] = \frac{2}{L} \sum_l l \frac{d}{dt}[\langle \hat{n}_l \rangle]. \quad (\text{S24})$$

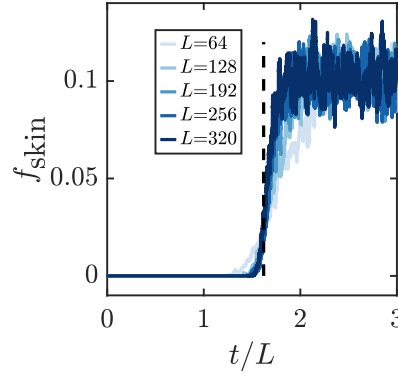


FIG. S1. The time evolution of the probability of finding the evolving state  $|\psi_t\rangle$  in the many-body skin state  $|\psi_{\text{skin}}\rangle$  averaged over trajectories in the presence of quasidisorder with  $W = 1$  ( $f_{\text{skin}} = [\langle\langle\psi_{\text{skin}}|\psi_t\rangle|^2]$ ). The black dashed line highlights the dynamical phase transition point in Fig. 3(b) in the main text.

Here,  $[\langle\hat{n}_l\rangle] = \text{Tr}(\rho_t \hat{n}_l)$  ( $[\cdots]$  denotes the trajectory average) where  $\rho_t$  is the density matrix that evolves based on the master equation

$$\frac{d\rho_t}{dt} = -i\hat{H}_{\text{eff}}\rho_t + i\rho_t\hat{H}_{\text{eff}}^\dagger + \gamma \sum_m \hat{L}_m \rho_t \hat{L}_m^\dagger. \quad (\text{S25})$$

Thus, we obtain

$$\frac{d}{dt}[\langle\hat{n}_l\rangle] = -i[\langle\hat{n}_l\hat{H}_{\text{eff}}\rangle] + i[\langle\hat{H}_{\text{eff}}^\dagger\hat{n}_l\rangle] + \gamma \sum_m [\langle\hat{L}_m^\dagger\hat{n}_l\hat{L}_m\rangle]. \quad (\text{S26})$$

Since each trajectory has the Slater determinant form, we can apply the Wick's theorem, e.g.,  $\langle\hat{c}_i^\dagger\hat{c}_j^\dagger\hat{c}_m\hat{c}_n\rangle = \langle\hat{c}_i^\dagger\hat{c}_n\rangle\langle\hat{c}_j^\dagger\hat{c}_m\rangle - \langle\hat{c}_i^\dagger\hat{c}_m\rangle\langle\hat{c}_j^\dagger\hat{c}_n\rangle$  and write  $v(t)$  in terms of two-point correlation functions,

$$v(t) = \frac{2}{L} \sum_{l=1}^L \left\{ i\text{l} \left[ \langle\hat{H}_{\text{eff}}^\dagger\hat{n}_l\rangle - \langle\hat{n}_l\hat{H}_{\text{eff}}\rangle \right] + l \sum_m \left[ \frac{1}{2}(\delta_{lm} + \delta_{l,m+1})\gamma\langle\hat{d}_m^\dagger\hat{d}_m\rangle - \langle\hat{n}_l\rangle i\langle\hat{H}_{\text{eff}}^\dagger - \hat{H}_{\text{eff}}\rangle - \gamma\langle\hat{d}_m^\dagger\hat{c}_l\rangle\langle\hat{c}_l^\dagger\hat{d}_m\rangle \right] \right\}, \quad (\text{S27})$$

where the term  $\langle\hat{H}_{\text{eff}}^\dagger\hat{n}_l\rangle$  can be calculated by

$$\sum_{i,j} \left[ H_{\text{eff}}^\dagger \right]_{ij} \langle\hat{c}_i^\dagger\hat{c}_j\hat{n}_l\rangle = \sum_{i,j} \left[ H_{\text{eff}}^\dagger \right]_{ij} \left( \langle\hat{c}_i^\dagger\hat{c}_j\rangle\langle\hat{n}_l\rangle - \langle\hat{c}_i^\dagger\hat{c}_l\rangle\langle\hat{c}_l^\dagger\hat{c}_j\rangle + \delta_{jl}\langle\hat{c}_i^\dagger\hat{c}_l\rangle \right). \quad (\text{S28})$$

## S-2. DYNAMICAL PHASE TRANSITION WITH THE QUASIPERIODIC POTENTIAL

In the main text, we have demonstrated the dynamical phase transition in the presence of quasidisorder by showing the change in the entanglement scaling as time evolves. In this subsection, we present the probability of the evolving state  $|\psi_t\rangle$  being in the ideal many-body skin state, that is,  $f_{\text{skin}} = [\langle\langle\psi_{\text{skin}}|\psi_t\rangle|^2]$ , for different system sizes when the quasidisorder strength  $W = 1$  in Fig. S1. The figure illustrates that the probability suddenly rises across the transition point, similar to the case without disorder.

## S-3. THE DYNAMICS OF THE SYSTEM UNDER PBCS

In the main text, we have shown the existence of the dynamical phase transition for a system under OBCs that arises from the competition between the bulk dynamics and boundary skin effects. We have also shown that under OBCs, the entanglement entropy first increases and then declines to a steady value as time evolves for weak quasidisorder. We argue that the maximum entanglement entropy with respect to the quasidisorder strength  $W$  reveals the entanglement

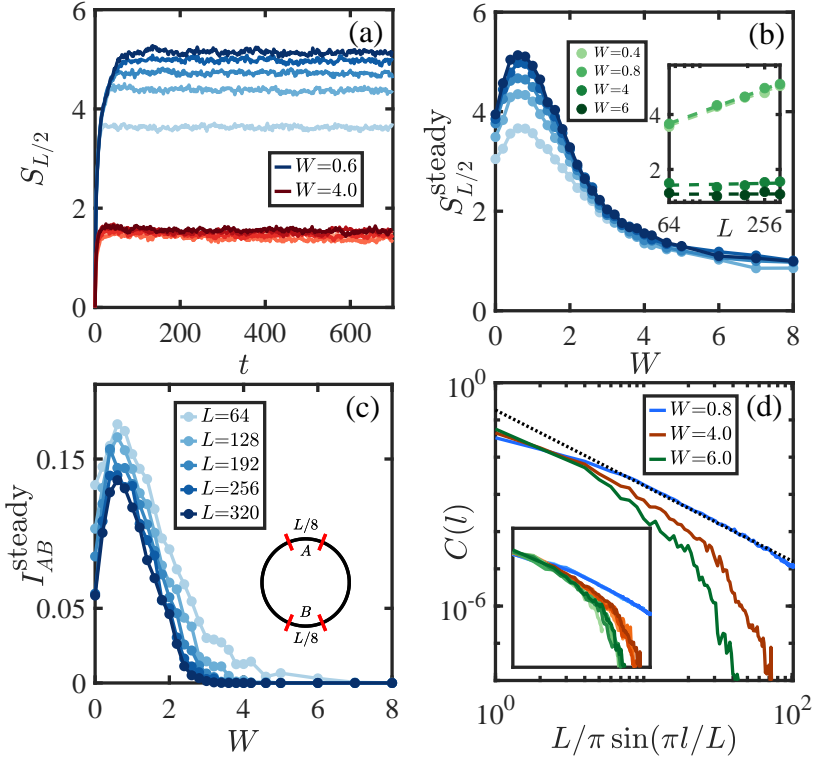


FIG. S2. The dynamics of the system under PBCs. (a) The time evolution of the trajectory averaged bipartite entanglement entropy  $S_{L/2}$  for system sizes  $L = 64, 128, 192, 256, 320$  (light to dark colors) at  $W = 0.6$  (blue lines) and  $W = 4$  (red lines). (b) The steady-state value of  $S_{L/2}$  with respect to the quasidisorder strength  $W$  for different system sizes. Inset: the linear-log plot of the steady-state value of  $S_{L/2}$  versus  $L$  at different  $W$ . (c) The trajectory averaged mutual information between two subsystems  $A$  and  $B$  (see the inset) for the steady state with respect to  $W$ . (d) The correlation function  $C(l)$  of the steady state with respect to  $(L/\pi) \sin(\pi l/L)$  for different  $W$ , with  $L = 320$ . The inset shows the data collapse of  $C(l)$  for  $L = 64, 128, 192, 256, 320$ .

transition of the steady state of the dynamics under PBCs. In this section, we will provide the results of the dynamics under PBCs in Fig. S2 to support the argument. Figure S2(a) illustrates that as time progresses, the bipartite entanglement entropy rises rapidly, reaching a steady value, in stark contrast to the OBC case [see Fig. 4(a) in the main text]. The dynamical phase transition thus does not happen in the PBC case, which is consistent to the fact that the dynamical phase transition appears due to the competition between the bulk dynamics and boundary skin effects.

However, for the steady state, the numerical results suggest a phase transition of the entanglement entropy of the steady state from a log-law to an area-law scaling with respect to  $W$  as shown in Fig. S2(b) (see the inset for the change in the scaling), similar to the OBC case. In addition, the correlation function  $C(l)$  exhibits a power-law decay at weak quasidisorder and develops into the exponential decay at strong quasidisorder, which agrees well with the OBC case. These results strongly suggest that the phase transition of the maximum entanglement entropy present in the OBC case arises from the initial bulk dynamics.

#### S-4. THE DYNAMICAL PHASE TRANSITION OF A SYSTEM WITH ONSITE DISORDER

In the main text, we have studied the dynamics of a system with quasidisorder. Since onsite disorder is ubiquitous, in this section, we will provide the results for a system with onsite disorder. To study the effects of onsite disorder, we introduce the term  $\sum_l m_l \hat{c}_l^\dagger \hat{c}_l$  in the Hamiltonian (1) in the main text, where  $m_i$  represents the onsite disorder that is uniformly sampled in  $[-W/2, W/2]$  ( $W$  now denotes the disorder strength rather than the quasidisorder one). In our numerical calculations, we average our results over 224-1000 sample configurations for one trajectory. In Fig. S3, we map out the phase diagram of the bipartite entanglement entropy with respect to  $t/L$  and  $W$ , showing the existence of a dynamical phase transition, similar to the case with quasidisorder. To explicitly illustrate the transition from

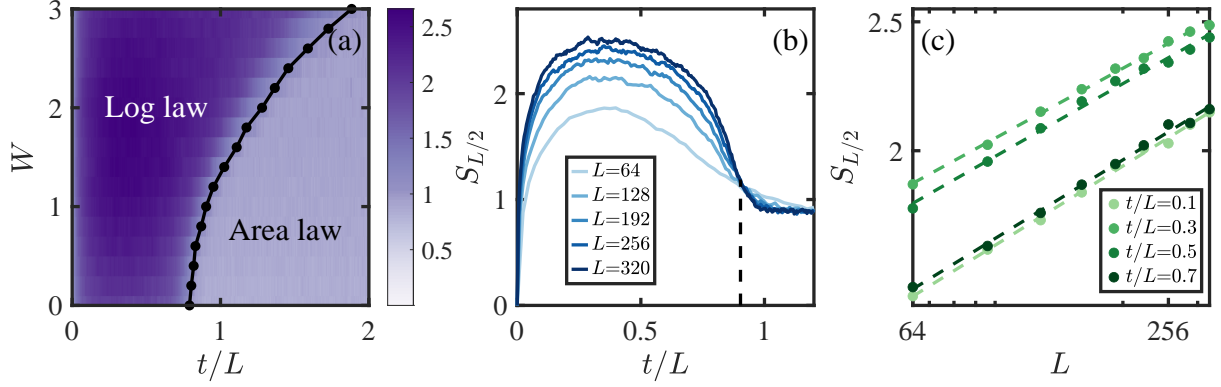


FIG. S3. The dynamics of the system with onsite disorder under OBCs. (a) The phase diagram of the trajectory averaged bipartite entanglement entropy with respect to  $W$  and  $t/L$  for the system with  $L = 320$ . The black dotted line represents the dynamical phase transition line, separating the log-law regime and the area-law regime. (b) The trajectory averaged bipartite entanglement entropy  $S_{L/2}$  as a function of  $t/L$  for different system sizes at  $W = 1$ . The black dashed line marks out the dynamical phase transition point. (c) The scaling of  $S_{L/2}$  with respect to  $L$  in a linear-log scale with  $L$  up to 320.

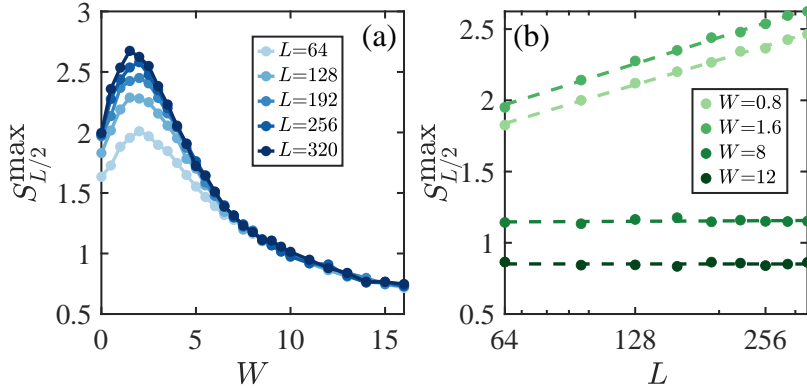


FIG. S4. (a) The maximum entanglement entropy with respect to the disorder strength  $W$  for different system sizes under OBCs. (b) The scaling of  $S_{L/2}^{\max}$  with  $L$  for several disorder strengths.

the log-law growth to an area-law behavior, we plot the time evolution of  $S_{L/2}$  in Fig. S3(b). It exhibits an increase-decrease-steady pattern, which closely resembles the quasidisorder case. Additionally, we present the scaling of  $S_{L/2}$  before the transition point in Fig. S3(c) to demonstrate that  $S_{L/2}$  follows the log-law growth in that regime.

Furthermore, similar to the quasidisorder case, our numerical results suggest the existence of the phase transition for the maximum entanglement entropy  $S_{L/2}^{\max}$  from the log-law regime to the area-law regime with respect to the disorder strength in the disordered system as shown in Fig. S4.